PNC-TN9410 88-151

In-Pile Experiment Analyses Relevant to Initiating-Phase Energetics

Nov., 1988

OARAI ENGINEERING CENTER

POWER REACTOR AND NUCLEAR FUEL DEVELOPMENT CORPORATION

複製又はこの資料の入手については，下記にお問い合わせください。
〒311-13　茨城県東茨城郡大洗町成田町4002
動力炉・核燃料開発事業団
大洗工学センター　システム開発推進部・技術管理室

Enquires about copyright and reproduction should be addressed to: Technology Management Section O-arai Engineering Center, Power Reactor and Nuclear Fuel Development Corporation 4002 Narita-cho, O-arai-machi, Higashi-Ibaraki, Ibaraki-ken, 311-13, Japan

動力炉・核燃料開発事業団（Power Reactor and Nuclear Fuel Development Corporation）

PNC-TN9410 88-151
November, 1988

In-Pile Experiment Analyses Relevant to Initiating-Phase Energetics

N. Nonaka*
F. Kasahara**
H. Niwa*
I. Sato*

ABSTRACT

For the safety assessment of LMFBRs, much effort has been devoted to the analyses of LOF accident sequences with an emphasis on initiating-phase (IP) energetics (LOF-d-TOP event). Important knowledge and experiences on the IP energetics have been accumulated through reactor studies and in-pile experiment analyses, typically for the CABRI experiments. The present paper summarises the current understanding of key phenomenology relevant to the IP energetics based on the CABRI experiment analyses and the validation study for the PAPAS-2S, SAS3D and SAS4A codes.

* FBR Safety Engineering Section, Safety Engineering Division, OEC
** FBR Safety Engineering Section, Safety Engineering Division, OEC
(presently with Nihon Atomic Industry Group, Inc.)

Contents

List of Tables

List of Figures

1. INTRODUCTION

The energetics potential in postulated core disruptive accidents (CDAs) has been one of major concerns in the safety of liquid-metal fast breeder reactors (LMFBRs), because the mechanical consequences may challenge the integrity of the reactor vessel (refs. 1, 2). On this subject, much effort has been devoted to the analyses of an unprotected loss-of-flow (LOF) accident sequences with an emphasis on the initiating-phase (IP) energetics.

This includes extensive reactor analyses with the SAS3D code (ref. 3) for a 700 MW(th)-class LMFBR with a homogeneous core design (ref. 2). Although the result exhibits relatively wide spectrum of sequences, the most probable sequence of the ULOF accident is energetically mild. An energetic accident progression, typically leading to a LOF-driven-transient-overpower (LOF-d-TOP) event, is found only when the pessimistic assumptions are superimposed such as: taking no credit for axial fuel expansion; using conservative reactivity coefficients; and suppressing an early fuel dispersive potential by fission gases.

This conclusion on the IP energetics makes a common basis with the other reactor studies for the moderate void-reactivity cores (refs. 1,4,5).

The energetic sequence, on the basis of conservatism, has been recognised to be an important issue for enveloping sufficiently phenomenological uncertainties and for confirming the safety margin to the vessel integrity.

The key phenomena in such upper-bound sequences are: (1) fuel dispersal in voided lead subassemblies (S/As); (2) fuel failure in partially- or un-voided S/As; and (3) resultant molten-fuel-coolant interactions (MFCIs).

For a realistic assessment of the energetics, therefore, these phenomena and the validity of relevant physical models must be investigated against experimental data simulating the high power and heating-rate condition (ref. 5).

In this respect, the CABRI in-pile experiments (ref. 6), which systematically cover various transient conditions with energetic power bursts, have provided valuable information

on the IP phenomenology.

An example of the characteristic test conditions is indicated in Fig. 1, where the fuel energy conditions for typical CABRI tests well represent the S/As approaching a LOF-d-TOP condition in the upper-bound reactor cases.

The several CABRI experiments have been selectively analysed to examine separately the above key phenomena with a suitable choice of the safety analysis codes PAPAS-2S (ref. 10), SAS3D and SAS4A (ref. 11). General characteristics for the tests studied are schematically explained in Fig. 2 with main transient conditions.

The present paper summarises the current understanding of key phenomenology and status of the code-validation studies based on the experiment analyses. Detailed information on the conditions and the results of the CABRI experiments are found in Refs. 6 - 9.

2. FUEL MOTION IN VOIDED CHANNEL

The fuel motion phenomenon in the lead S/As is very important in determining the possibility and severity of a LOF-d-TOP event and hence in assessing the IP energetics. In CABRI tests, energetic power pulses were triggered following the extended LOF conditions with channel voiding and cladding relocation. In these tests, an axially bi-directional dispersive fuel motion shortly after the initial fuel disruption was observed by a neutron hodoscope (ref. 8.)

To investigate the mechanisms and behaviour of the fuel motion, extensive experiment analyses have been performed. Among these, the results of SAS3D and SAS4A analyses of the B5 test, a typical LOF-d-TOP experiment with a fresh fuel pin, are described in the following. The phenomena specifically discussed include: coolant boiling and cladding relocation, fuel disruption, and fuel motion mechanisms.

Other experiments and analyses are also referred to when they are necessitated.

Coolant boiling and cladding relocation

It was shown that both SAS3D and SAS4A could successfully simulate the LOF boiling phase before the power burst. Generally

good agreements with measured data were obtained for evolution of the void and clad-melting boundaries (ref. 9). One example of comparisons with measured data is indicated in Fig. 3.

Figure 6(3) shows the coolant channel state at pulse triggering in the SAS4A analysis. Some molten cladding remains on the fuel and only partial blockages are formed, mainly because of a wide flow area in the test section. The SAS3D result in Fig. 3 shows the same trend which is fairly consistent to the measured flow response and the results of post-test examination for a simple LOF test B1.

Further, the temperature of the refrozen cladding was still close to the melting point of steel, and hence the flow path would be available for possible later fuel dispersal.

Fuel disruption

In the B5 test, the fuel disruption was observed at 58 ms into the pulse triggering, when the average fuel energy exceeded the liquidus point. This implies that the liquid fuel expansion was a main disruption mechanism for the fresh fuel.

The in-pile fuel-disruption experiment at Sandia (ref. 12) indicated that the mode of disruption is very sensitive to the fuel heating rate and that a high heating rate like in CABRI leads to a dispersive mode (liquid-spray or fine break) both for fresh and irradiated fuel. Such efficient fuel fluidisation may also promote mixing and heat exchange with the remaining molten steel.

After the fuel disruption, the fuel motion is governed by various pressure sources. Although the fuel vapour is dominant in an extremely energetic case, other sources, such as fission gas, steel and sodium vapour, are also available for driving the fuel motion.

Effect of fission gas on fuel motion

The effect of fission gas is noticed when the irradiated fuel test BI3 (1 % burnup) is compared with the fresh-fuel test B4. That is, the dispersive fuel motion was observed in BI3 with much lower fuel energy state than in B4.

Such an irradiation effect was also confirmed in the several TREAT in-pile tests (refs. 13,14). Hence the effect of fission gas

on the early fuel dispersal is acceptable, though the complex fission gas dynamics throughout the transient is still to be resolved.

Effect of steel vapour on fuel motion

It has been pointed out that the effect of steel vapour becomes important in an energetic LOF sequence, because the fuel and the cladding tend to co-disrupt in lead S/As without separate cladding relocation (refs. 1, 4).

The parametric analyses on the fuel motion phenomenon indicate clearly that fuel motion observed shortly after the disruption cannot be explained only by the fuel-vapour pressure, but by the contribution of the steel vapour pressure. The results of the parametric cases are depicted in Fig. 4, where the evolution of normalised fuel worths is shown to compare the overall trends of fuel motion. The dotted regions show the fuel worth change roughly estimated by correcting the averaged hodoscope data to bound the uncertainty in the self-shielding effect.

Case D with SAS4A was recognised to explain the observed phenomena most consistently. In Case C, the molten cladding only works as a heat sink, resulting in considerably slow fuel motion with delayed fuel vapourisation.

Case A with SAS3D, in which all the molten cladding is assumed to relocate and to form rigid blockages, is also unrealistic, considering the situation in Fig. 6(3). Case B was intended to calibrate the SLUMPY parameters effective for initial pressurisation, such as the fuel-to-steel mixing ratio and the heat-transfer rate. The results showed the comparative fuel behaviour with Case D, although more fuel penetrated into the blanket region because the interactions with intact structures were poorly modelled.

Figure 5 compares the calculated fuel distributions by SAS3D and SAS4A with the hodoscope data for the selected time intervals. The SAS3D result in the figure corresponds to a modified Case B with increased fuel viscosity, and the SAS4A result is adopted from Case D. The both cases well explain the global trend in the observed fuel motion.

Figure 6 exhibits the material-motion behaviour in Case D. In this analysis, the partial cladding blockage formed previously

is remelted by a contact with the hot fuel and then this influences the subsequent material motion. The temporary fuel accumulation around 65 to 75 ms observed by the hodoscope well explains this behaviour.

In the test, further upward fuel motion is followed, indicating the highly dispersive potential. These extended fuel behaviours, however, are not realistically treated by SAS3D. For instance, the analysis in Fig. 5 results in a complete stoppage of the upper moving front.

Effect of sodium vapour on fuel motion

The initial dispersive fuel motion up to around 70 ms was controlled by pressure generation inside the disrupted region, and the later motion was affected by possible interactions of the liquid fuel with the other materials near the relatively cold regions.

In the lower region near the sodium interface, an interaction between the molten materials with the sodium slug was observed, possibly because of a relatively short distance between the liquid slug and the disrupted fuel region. This phenomenon was also simulated in the SAS4A analysis shown in Fig. 6(5-8).

Careful examination of the SAS4A analysis suggests that its prompt effect on fuel motion is rather localised near the interacting region, because it cannot change the pressure gradient which has been developed by steel vapourisation. Nevertheless, the sodium vapourisation plays an important role in driving the later dispersive fuel motion.

The above discussions conclude that the steel vapour increases the disrupted-region pressure sufficiently to cause an early fuel dispersal under an energetic power burst condition, and that the sodium vapour generated at the lower interface may potentially enhance the fuel dispersal. The both mechanisms are closely linked to the disruption mode and pre-overpower channel state which determine the mixing condition of core materials.

SAS4A has revealed its advanced capabilities for realistic analyses of the experiments. SAS3D, in which the fuel motion is modelled more parametrically, is also recognised to be quite valuable especially in a conservative analysis if the model parameters are

selected properly.

3. FUEL-PIN RESPONSE UP TO FAILURE

The thermo-mechanical response of a fuel pin subjected to a CABRI transient was analysed by the PAPAS2S code. The code has been developed at PNC aiming at detailed examinations of the fuel-pin failure mechanism and resultant MFCI phenomena in an unvoided or partially voided channel. The code is also used for reactor analyses to support the SAS3D and SAS4A codes.

The analytical models for the fuel-pin deformation and MFCI are based on DEFORM-II (ref. 15) and EULFCI (ref. 16), respectively, and the coolant boiling is treated by a multi-bubble, slug-ejection model.

In the experiment analyses, the data obtained from PIE and the material properties of the sibling and test pins are also taken fully into account for precise analytical condition.

Axial fuel expansion

A comparison between the experimental data and the PAPAS-2S analyses for the various CABRI tests shows that almost free expansion of a fuel stack is expected at least until a tight contact between the fuel pellets and cladding occurs. Also indicated is that the stick formation under an overpower condition considerably reduces the expansion depending on the initial gap size and the axial extent of the contact.

Figure 7 compares the calculated and measured fuel expansion during the LOF phase in the B4 and BI3 tests. Pre- and post-boiling thermal responses of the fuel well explain the measured expansion behaviour.

Therefore, the fuel expansion is effective during the pre-overpower LOF phase in which the open gap condition over a wide axial region is maintained or encountered by cladding heatup. This contributes to a negative reactivity feedback in a LOF accident in an LMFBR.

Fuel-pin failure

The fuel-pin failure condition relating to the LOF-d-TOP event is crucial in assessing the IP energetics. In particular, the assumption of an imposed midplane failure with a low energy threshold often augments drastically the energetics level.

The CABRI experiments, simulating various coolant conditions before the power burst, have provided valuable data on this issue. Based on the five I-series CABRI experiments (AI2, AI3, BI2, BI4 and BI6), the average peak enthalpy of fuel at pin failure was evaluated to be 1.35 ± 0.05 kJ/g and the average relative height of the failure positions was 0.64 ± 0.06.

The failure energy is obviously higher than that obtained in the E- and HUT-series TREAT experiments (ref. 1). This implies an important effect of the fuel heating rate on the failure threshold. Figure 8 indicates the relationship between fuel failure energies and fuel heating rates for the TREAT and CABRI experiments. Namely, the energy deposition rates in CABRI are an-order-of-magnitude higher than in TREAT, and more adiabatic heating in CABRI seems to have enhanced the failure energy.

In spite of such a high energy-deposition rate with a relatively high axial power peaking (1.33), the initial failure sites were located above the midplane, especially in the LOF-d-TOP tests. This suggests a considerable effect of the cladding temperature profile determined by the coolant condition.

Based on the PAPAS-2S analyses, the basic failure mechanism of the fuel pin in CABRI is characterised by the fuel-pin cavity pressurisation by molten fuel with the cladding strength deteriorated by an elevated temperature level. This then determines the cladding strain behaviour, including the axial profile and the stain rate, and finally causes the fuel-pin failure.

Figure 9 depicts the transient cladding strain behaviour at the failure position predicted by PAPAS-2S. As seen in the figure, the failure occurs during the unloading phase of a pellet-cladding mechanical interaction, and coincides with the timing of increasing strain rate due to the cavity pressurisation under the elevated cladding temperature condition.

The cavity pressurisation is affected by several features,

such as the fuel-pin characteristics (fuel density, fission-gas retention, gap size, etc.), the extent of fuel-melting progression and the axial fuel expansion.

The sensitivity study by PAPAS-2S revealed that the initial fuel-cladding gap size and the axial fuel expansion potential play important roles in determining an available cavity volume to accommodate the internal pressure.

The fuel pins used in the I-series tests had narrow gaps (ca. 10μm at cold condition) and resulted in a limited axial expansion during the transient. A larger gap size (ca. 60μm) in the AH3 test, due to the irradiation clad swelling, resulted in a much higher failure energy (1.65 KJ/g). In spite of the high burnup condition (4.8 %), the failure threshold was comparable with the results of the fresh-fuel tests. These findings may explain the above arguments.

As shown in Fig. 10, the observed failure sites clearly correspond to the peak strain nodes in the analyses. The axial strain profile is influenced also by the coolant condition at the power burst. That is, the preceding LOF phase in BI2 (unvoided), BI4 and BI6 (partially voided) makes the upper cladding temperature distribution higher (more than 1000 °C) and flatter. Thus the possibility of the above-midplane failure is further increased.

Also indicated in Fig. 10 is that the high cladding strain develops over a wide length, particularly in the LOF-d-TOP cases. This, together with the high cladding temperature level and the extended fuel melting, implies a potential of axial failure propagation. This potential might be supported by the fact that two failure sites were observed in the most energetic test BI6. Therefore, the fixed failure site at the core midplane, postulated in conservative reactor analyses, seems unrealistic under the LOF-d-TOP condition.

With respect to the criteria to predict fuel-pin failure, the life-fraction rule (ref. 17) with Larson-Miller parameters is found to be most applicable, since this reasonably reflects the actual loading mechanism of the cladding mentioned previously.

The failure times and positions predicted by this criterion are compared with the experimental results in Table 1. Overall

agreements are good except for somewhat delayed failure predicted in the least energetic test BI4.

It has been confirmed through the extensive experiment analyses that PAPAS-2S, incorporating the above criterion, is highly useful for predicting the fuel-pin failure in LOF-d-TOPs.

4. MFCI IN UNVOIDED CHANNEL

The MFCI phenomena in an unvoided channel in the AI3 and BI2 tests were analysed by SAS3D and PAPAS-2S. The test pins were subjected to almost the same energy deposition during a TOP phase, and BI2 was preceded by a LOF phase.

Coolant dynamics

In both the tests, rapid fuel ejection and flow expulsions (see Fig. 12) were observed upon the fuel-pin failure. This may also result from the failure mode, discussed above, under high cavity pressure and extended fuel melting.

Based on the analyses, this initial flow acceleration was caused first by the channel pressurisation due to fuel and fission-gas ejection, and then by sodium vapourisation from MFCIs. The fuel-to-sodium heat transfer seems to be highly efficient. That is, the mixing and fragmentation time constant in the Cho-Wright heat-transfer model is very small (less than 1 ms) to simulate the above flow behaviour, when a fuel particle diameter of 150 - 400 μm is used. This could be explained by the hydrodynamic fragmentation process, because the initial fuel ejection velocity was predicted to be very high (several 10 m/s) as a result of the high fuel-pin internal pressure.

Following the short-term slug acceleration, the interaction zone further expanded with sodium vapourisation. As shown in Fig. 11, the nominal SAS3D case tends to overestimate the expansion. Because the interaction zone in SAS3D is treated uniformly (namely, fuel and coolant mass and temperature distributions are smeared), the resultant coolant heat-up is overestimated. A reduction of the heat transfer in this period of MFCI gave a better agreement with the experiment (see the best-estimate case in Fig. 11).

In the PAPAS-2S analysis in which the interaction zone is

treated more in detail, the zone expansion as well as the flow response was better reproduced with the same heat-transfer model (see Figs. 11 and 12).

Regarding the LOF effect on MFCI, BI2 revealed less violent flow response than AI3. This is mainly because the small coolant subcooling in BI2 resulted in an earlier boiling onset and reduced the fuel-to-sodium heat transfer due to the effect of vapour blanketing.

Fuel motion

As discussed previously, the possibility of failure propagation becomes higher under an energetic LOF-d-TOP condition. In the BI2 test, failure extension was observed by the hodoscope, though the event occurred relatively slowly.

This phenomenon was simulated with PAPAS-2S by modelling a delayed failure-rip extension toward the both axial directions, i.e. 20 cm downward and 10 cm upward. The fuel motion behaviour in this analysis is shown in Fig. 13. Compared with the fixed failure condition, it was found that the extended-failure condition considerably alleviates fuel accumulation near the failure site and promotes upward fuel motion, showing a better agreement with the hodoscope data.

The normalised fuel worth behaviours in the above analyses are shown in Fig. 14. It is confirmed that the effect of the failure extension on the fuel dispersal is very important.

Also shown in Fig. 14 is the result of a SAS3D analysis. Though the initial worth change is slightly larger, the later fuel motion in SAS3D is less dispersive than the results by PAPAS-2S. This difference again resulted from the simple modelling of the interaction zone in SAS3D. Namely, a large amount of fuel ejected during decompression phase in the MFCI zone is hardly accelerated in SAS3D, while PAPAS-2S models the momentum coupling between fuel particles and flowing vapour, resulting in a more dispersive fuel behaviour.

It should be noted that the above non-dispersive characteristics of the SAS3D model is further enhanced in combination with the over-compactive in-pin motion if the failure site approaches the core midplane.

It is therefore concluded that SAS3D potentially gives conservative results from the viewpoint of the MFCI phenomenon under energetic power burst conditions.

5. CONCLUSIONS

The CABRI experiment analyses presented in this paper have significantly improved the understanding of the key phenomena relevant to the IP energetics. In particular, it is confirmed as a general trend that the dispersive potential of post-failure fuel motion is enhanced by the several mechanisms being effective in LOF-d-TOP events. Further, this potential is tightly related to the fuel failure modes dominated by the energetic power burst conditions.

The validity and applicability of the PAPAS-2S, SAS3D and SAS4A codes were intensively examined with supports of the highly qualified experimental data. The current status of the experiment analyses indicates that the SAS3D code is quite valuable especially in a conservative assessment of the IP energetics, and that the PAPAS-2S and SAS4A codes are capable of analysing realistically the key phenomena and are effective in providing complementary information for the SAS3D analysis.

ACKNOWLEDGMENT

The authors would like to express their gratitude to the members of the CABRI Project for their excellent work on the in-pile experiments. Especially, the hodoscope team has provided valuable information on the transient fuel behaviours frequently referred to in this study.

The authors also acknowledge the staff of the Reactor Safety Section, PNC for their direct or indirect contributions to this study.

The SAS3D and SAS4A codes were introduced from the Argonne National Laboratory under the agreement with the U. S. Department of Energy.

REFERENCES

1. THEOFANOUS T.G. and BELL C.R. An assessment of CRBR core disruptive accident energetics. NUREG/CR-3224, LA-9716-MS, 1984.

2. NAKAI Y. et al. Safety aspects in the design of "MONJU". Proc. LMFBR Safety Topical Meeting, Lyon, Ecully, 1982

3. CAHALAN J.E. and FERGUSON D.R. A preliminary user's guide to Version 1.0 of the SAS3D LMFBR accident analysis computer code. Argonne National Laboratory, 1977.

4. ROYL P. et al. Analysis of hypothetical loss-of-flow accidents without scram in the SNR-300 end-of-life Mark 1A core using the SAS3D code system. Proc. Int. Mtg. on Fast Reactor Safety Technology, Seattle, Washington, 1979.

5. MORRIS E.E. et al. Unprotected LOF in the CDS phase II heterogeneous reactor: initiating phase. Trans. Am. Nucl. Soc. 39, p.660, 1981.

6. DADILLON J. et al. CABRI Project - recent progress and present status. Proc. LMFBR Safety Topical Meeting, Lyon, Ecully, 1982.

7. KUSSMAUL G. et al. The CABRI project - overall status and achievements. Proc. Int. Mtg. on Science and Technology of Fast Reactor Safety, Vol 1, p.103, Guernsey, 1986.

8. BAUMUNG K. et al. Fuel motion measurements with the CABRI hodoscope. Proc. Int. Mtg. on Science and Technology of Fast Reactor Safety, Vol 1, p.141, Guernsey, 1986.

9. NISSEN K.L. et al. Interpretation of selected CABRI loss-of-flow experiments. Proc. Int. Mtg. on Science and Technology of Fast Reactor Safety, Vol 1, p.115, Guernsey, 1986.

10. Annual Report on FBR Safety R&D Program at PNC (JFY 1983). PNC SN943 84-06, p.38, 1984.

11. TENTNER A.M. et al. The SAS4A LMFBR whole core accident analysis code. Proc. Int. Mtg. on Fast Reactor Safety, Knoxville, Tennessee, 1985.

12. WRIGHT S.A. et al. In-pile determination of disruption mechanisms under LMFBR loss-of-flow accident conditions. J. Nucl. Tech. 71, p.326, 1985.

13. SIMMS R. et al. Loss-of-flow transient reactor test facility tests L6 and L7 with irradiated liquid-metal fast breeder reactor type fuel. J. Nucl. Tech. 52, p.331, 1981.

14. BAUER T.H. et al. TUCOP tests LO4 and LO6: comparison of irradiated and fresh fuel. Trans. Am. Nucl. Soc. 47, p.248, 1984.

15. WATANABE A. The DEFORM-II: mathematical analysis of elastic, viscous and plastic deformations of a reactor fuel pin. ANL-8041, 1973.

16. SHIMEGI N. EULFCI code: numerical method for coolant dynamics in one dimension. J. Nucl. Sci. Tech. 16(12), p.869, 1979.

17. MAST P.K. and SCOTT J.H. Fuel pin failure models and fuel-failure thresholds for core disruptive accident analysis. Proc. Int. Mtg. on Fast Reactor Safety and Related Physics, Chicago, Illinois, 1976.

Table 1. Comparison of failure time and position between experiments and analyses
* relative fuel height

Test ID	Time (ms) exp.	PAPAS-2S	Position* exp.	PAPAS-2S
AI3	82	85	0.59±0.04	0.57±0.03
BI2	79.5	80.5	0.67±0.07	0.67±0.07
BI4	88	94	0.63±0.06	0.60±0.07
BI6	63	63	0.73, 0.55	0.70±0.03

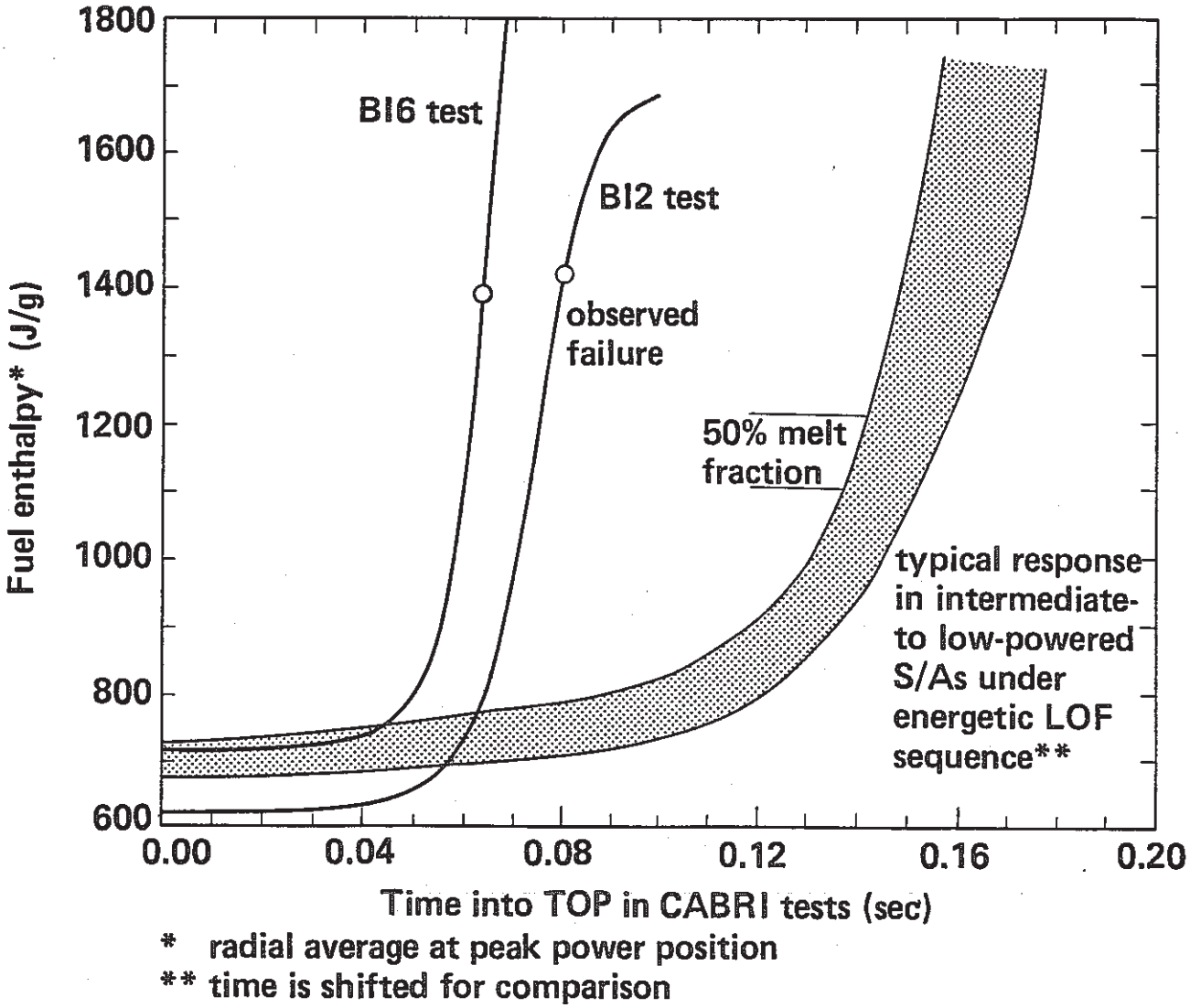

Fig. 1 Fuel energy histories in LOF—d—TOP CABRI tests and energetic reactor condition

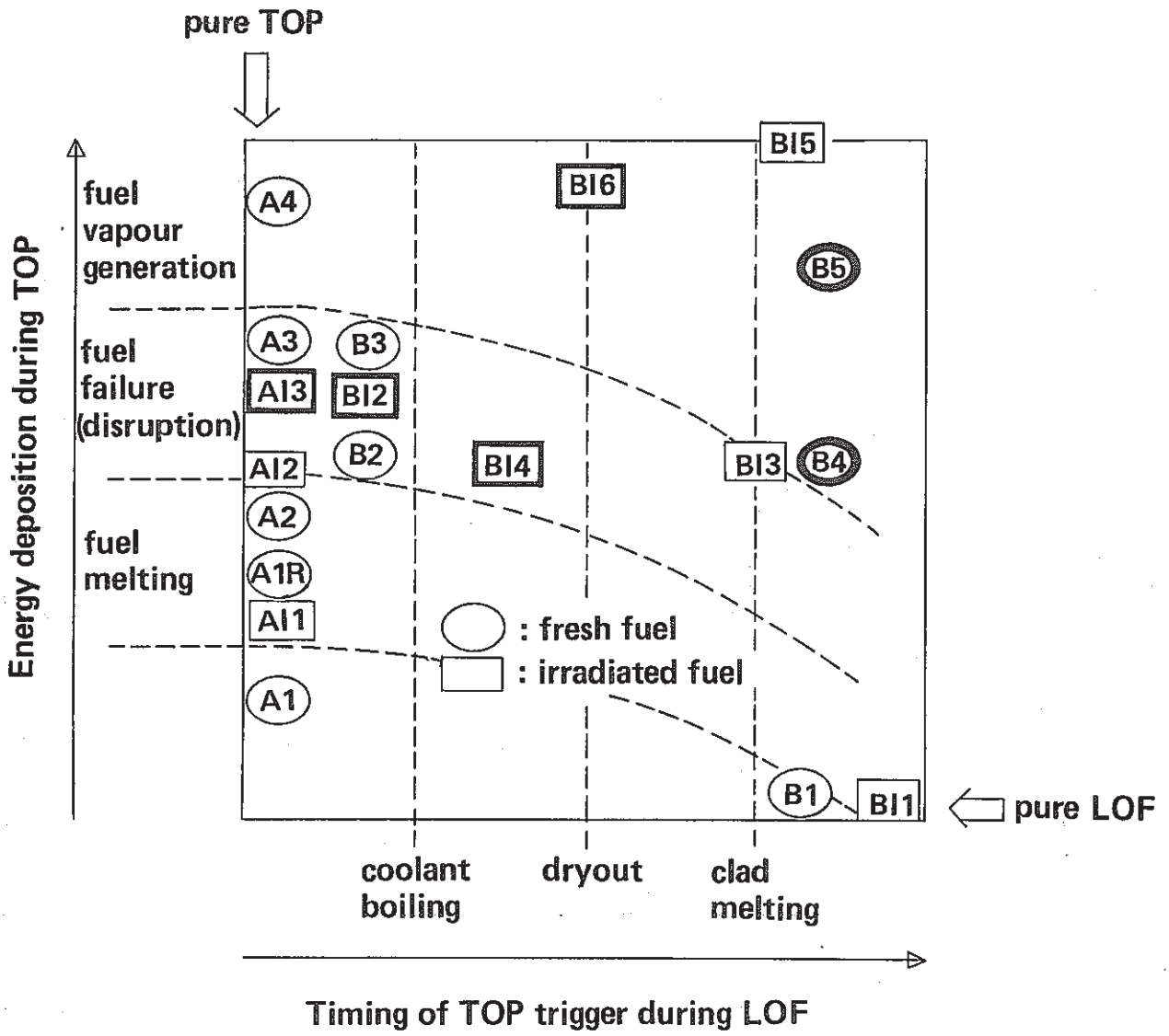

Fig. 2 Phenomenological expression of CABRI test matrix (fresh and low burn-up series)

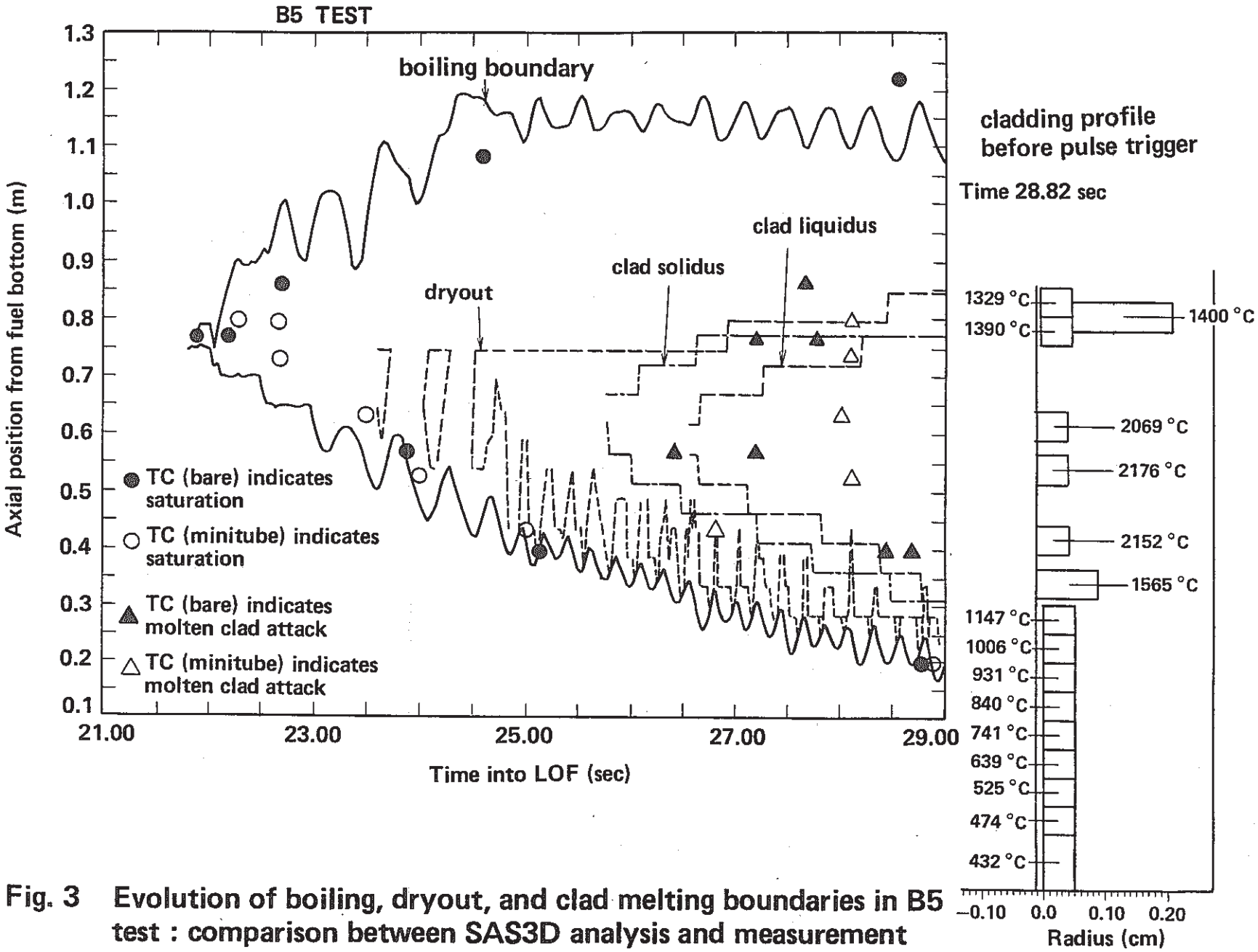

Fig. 3 Evolution of boiling, dryout, and clad melting boundaries in B5 test : comparison between SAS3D analysis and measurement

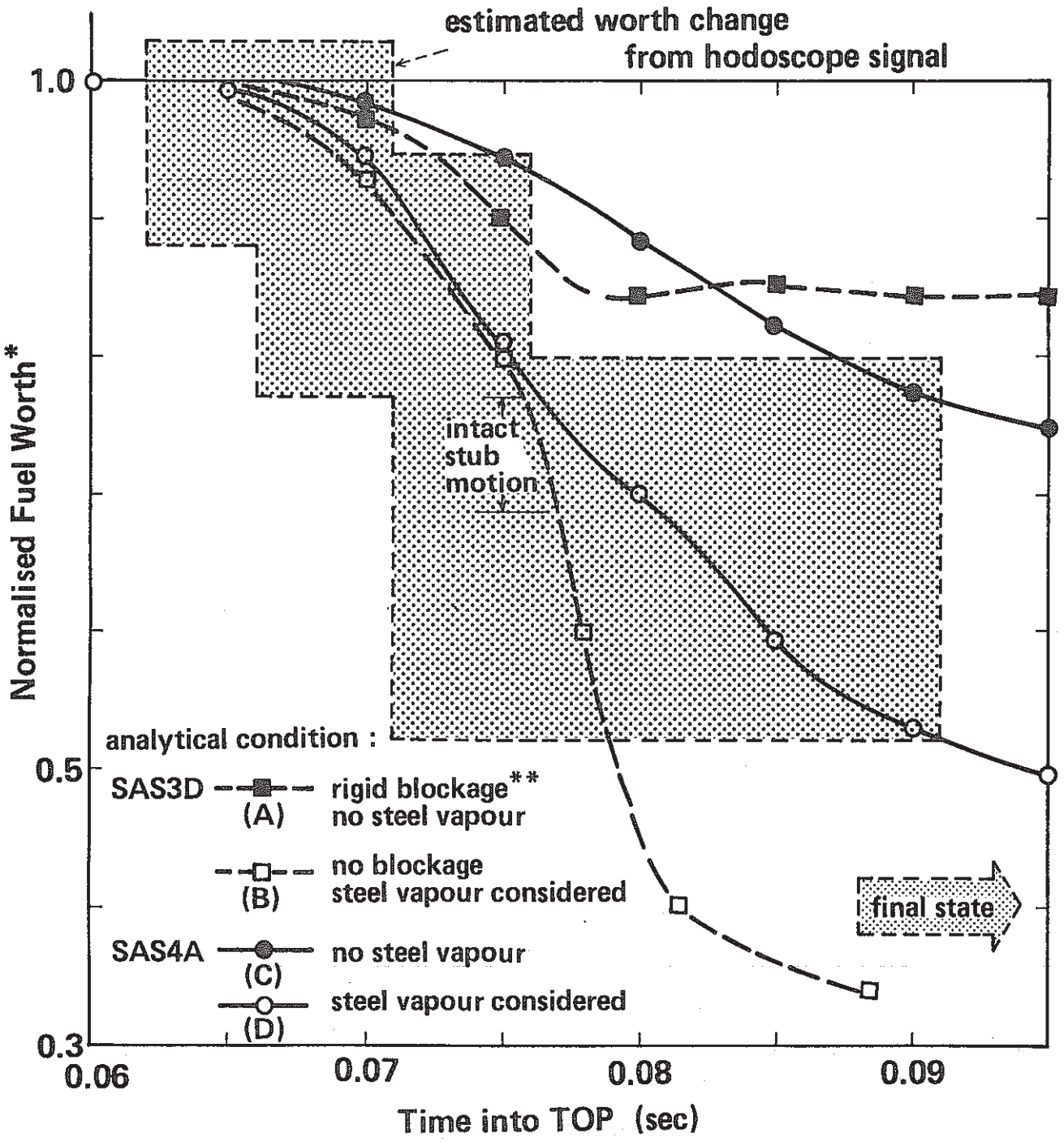

Fig. 4 Histories of fuel worth change in fuel motion analyses of B5 test

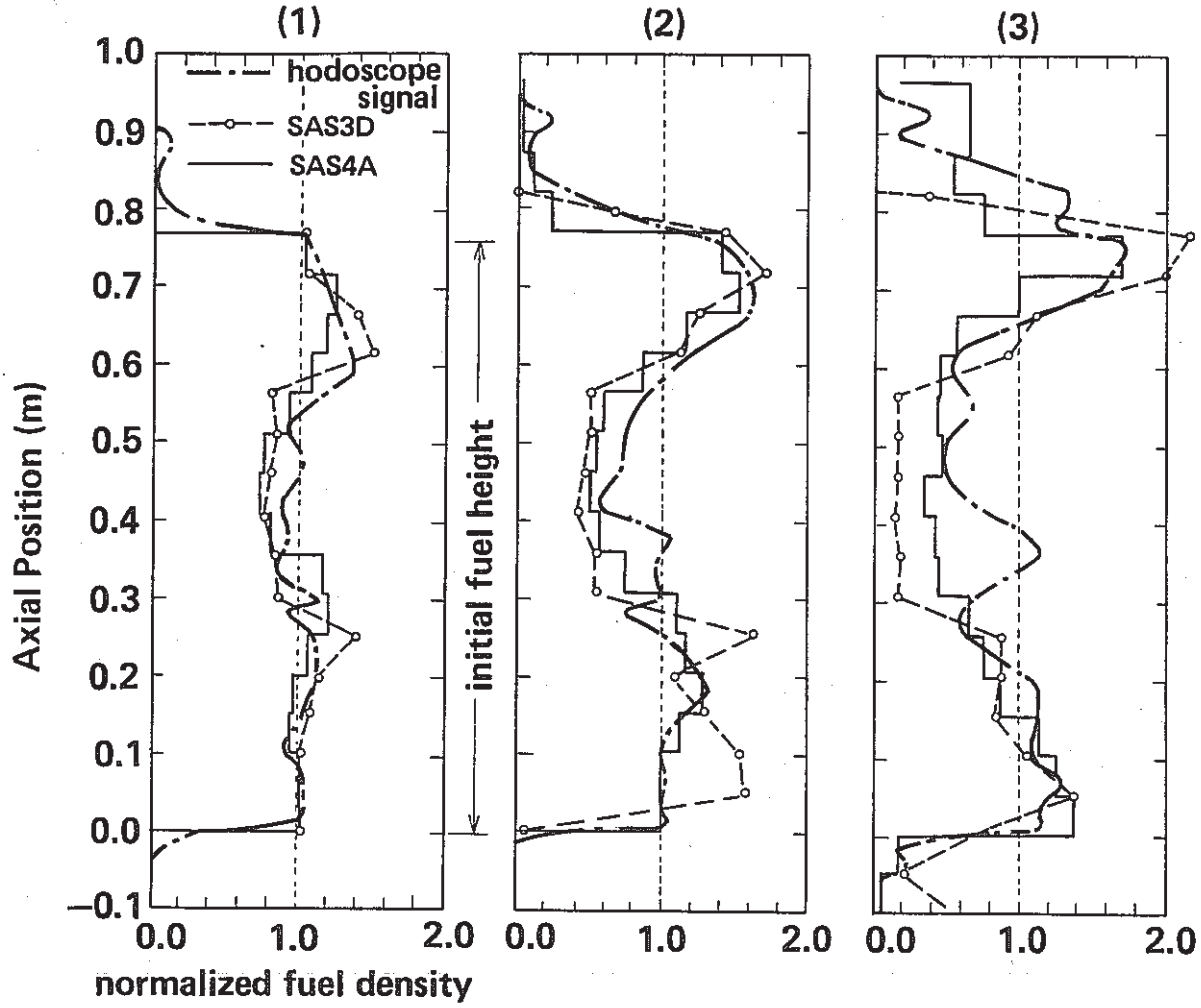

Time into TOP (after breakup)	58 ~ 68 ms (5 ± 5 ms)	63 ~ 73 ms (10 ± 5 ms)	68 ~ 78 ms (20 ± 10 ms)

* hodoscope data and analytical results are averaged in each time interval

Fig. 5 Axial fuel distributions for selected time intervals* in B5 test analyses by SAS3D and SAS4A

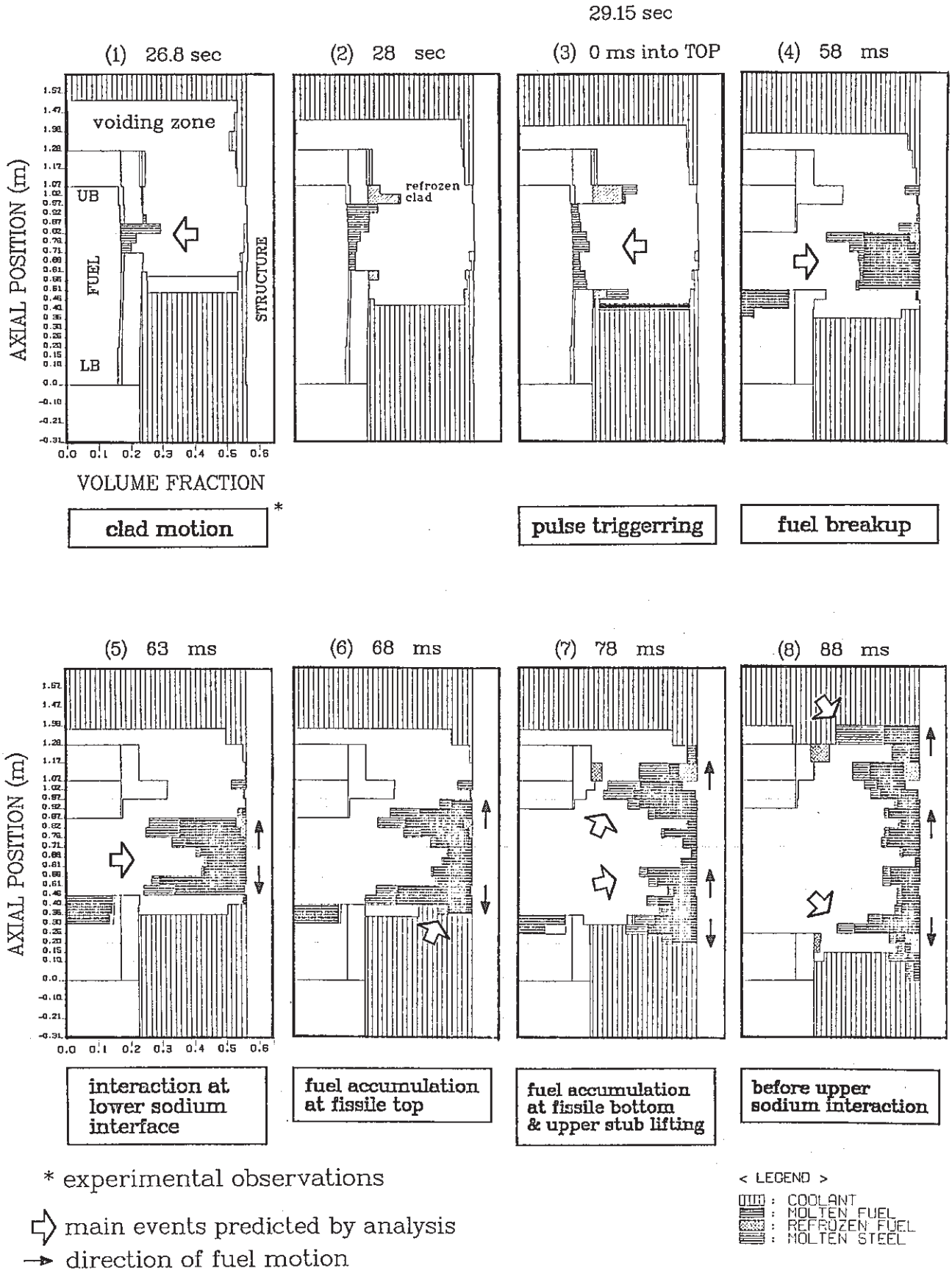

Fig. 6 Material Motion History in B5 SAS4A Analysis

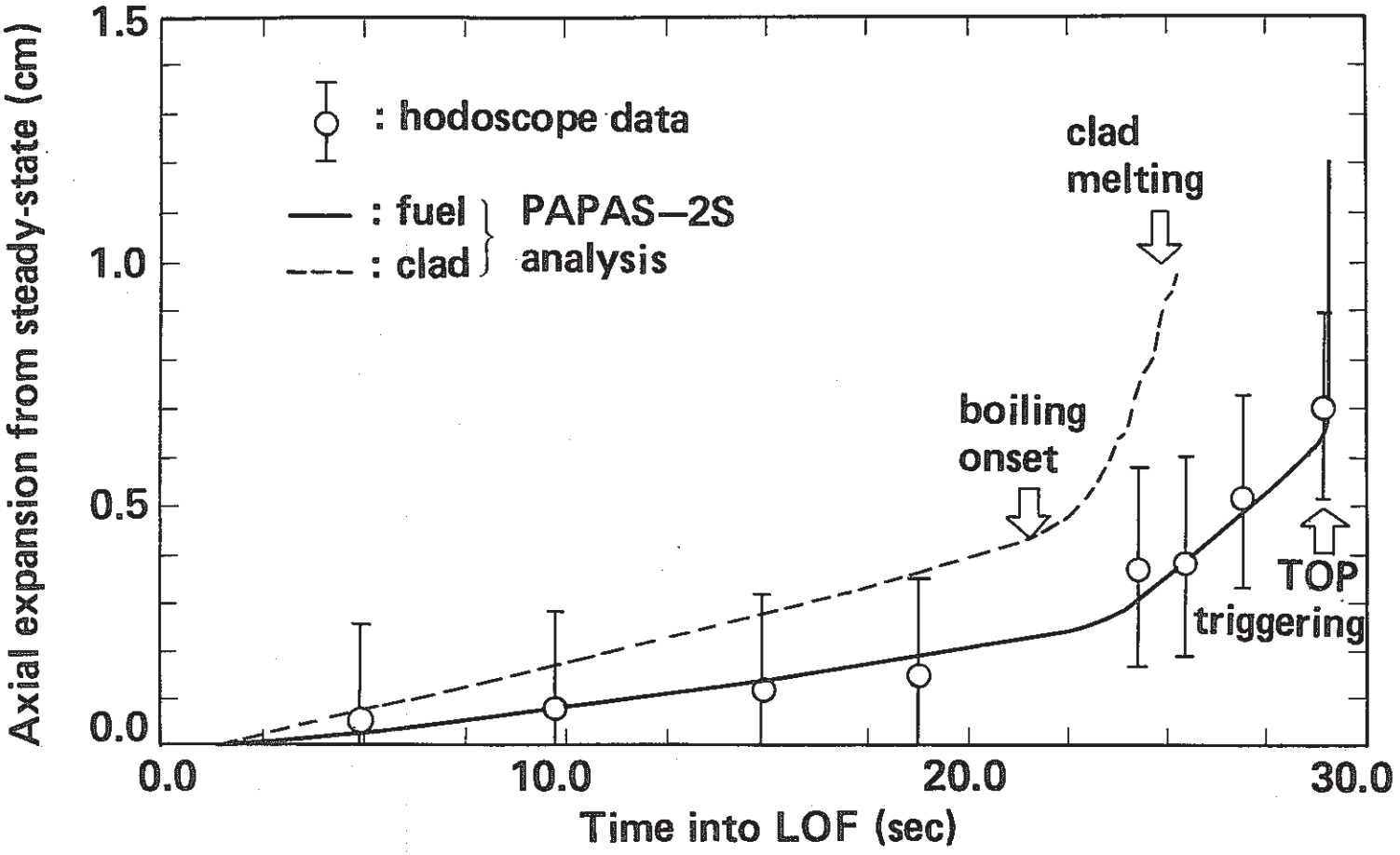

Fig. 7(1) Axial fuel expansion during LOF phase in B4 test

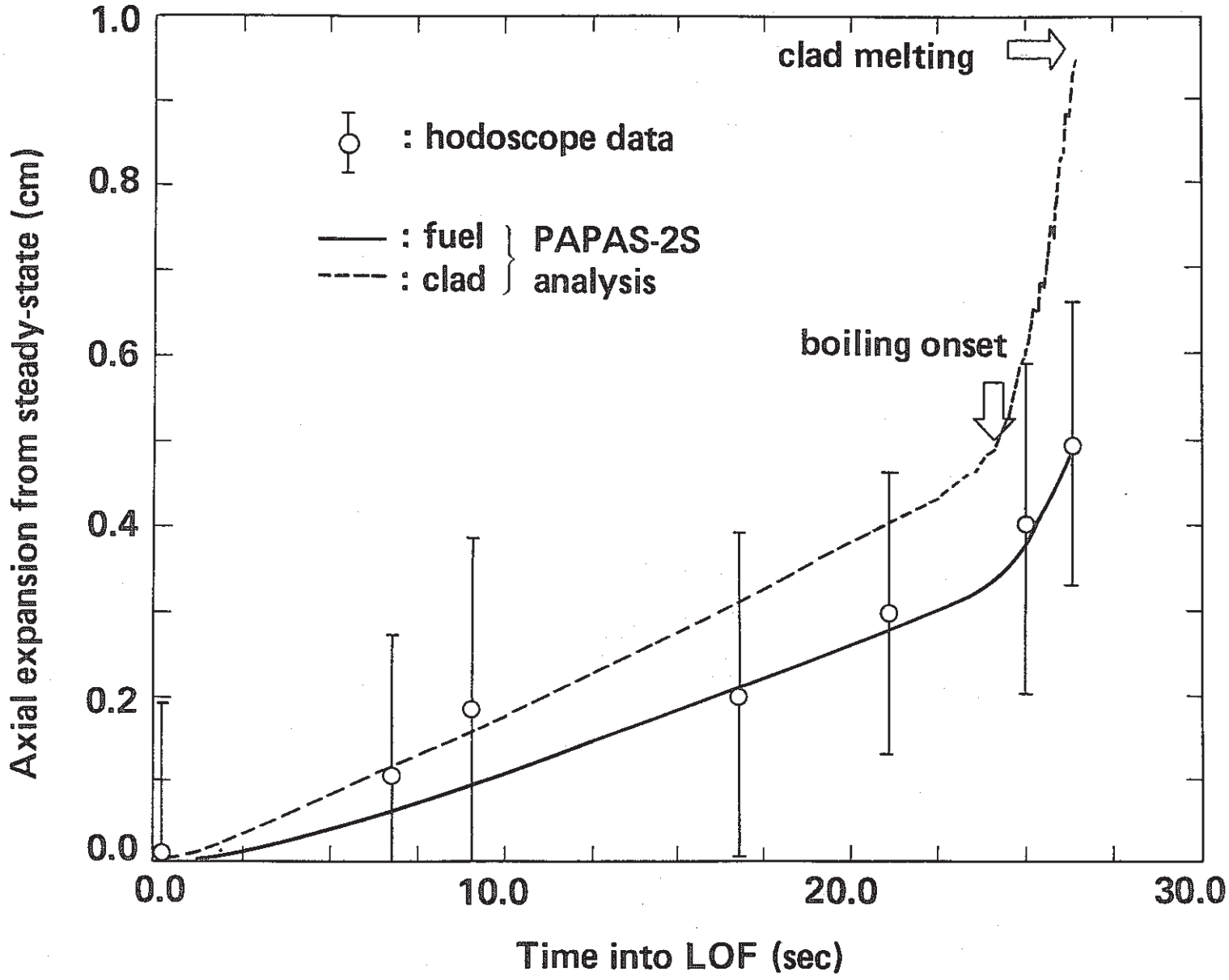

Fig. 7(2) Axial fuel expansion during LOF phase in BI3 test

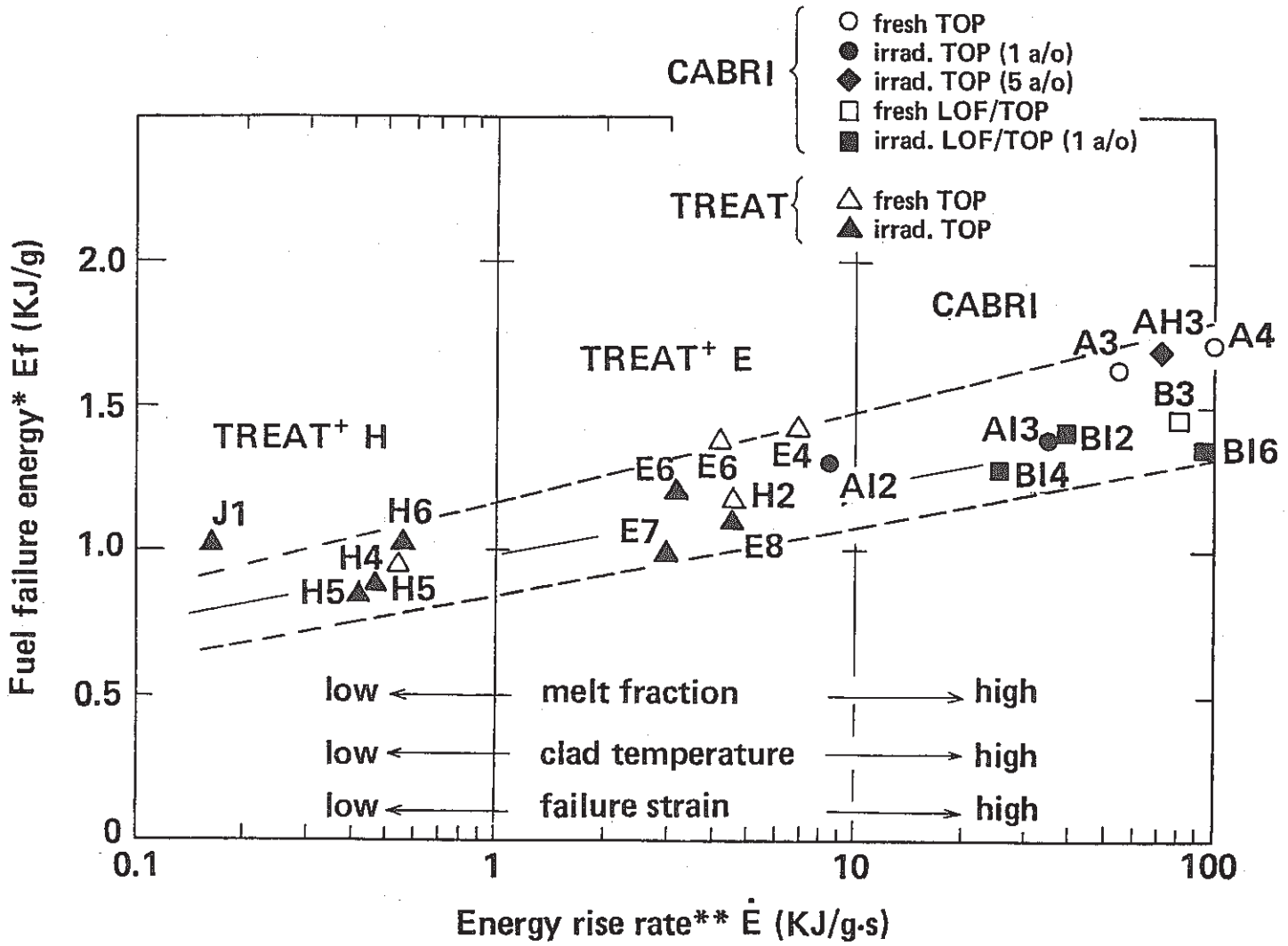

Fig. 8 Relationship between fuel failure energy and energy rise rate for coolant —restrained type tests in TREAT and CABRI

* radial averge at peak power position
** estimated around failure time
\+ flowing Na loop, SS316 clad, solid pellet

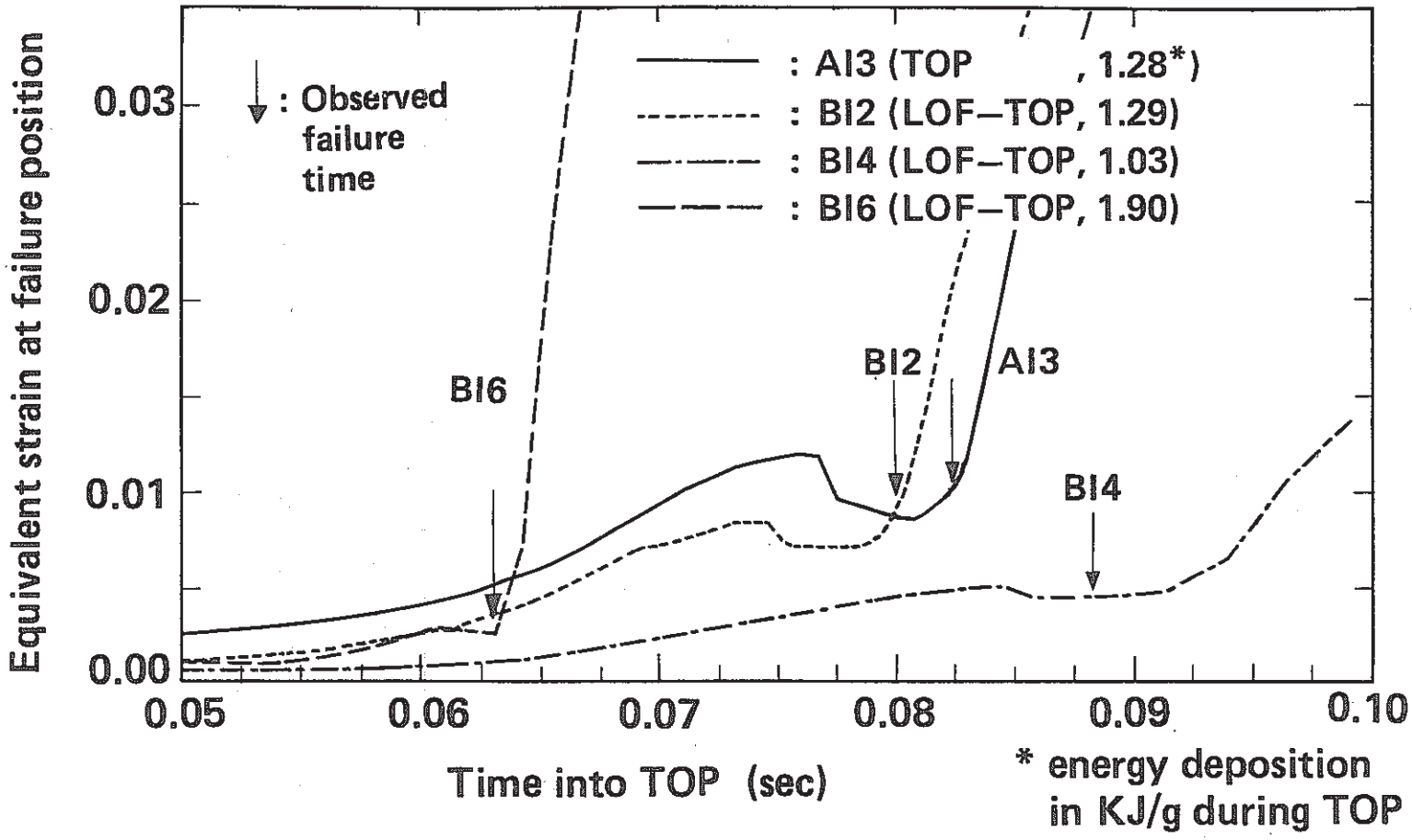

Fig. 9 Transient cladding strain behaviour predicted by PAPAS-2S and observed failure time

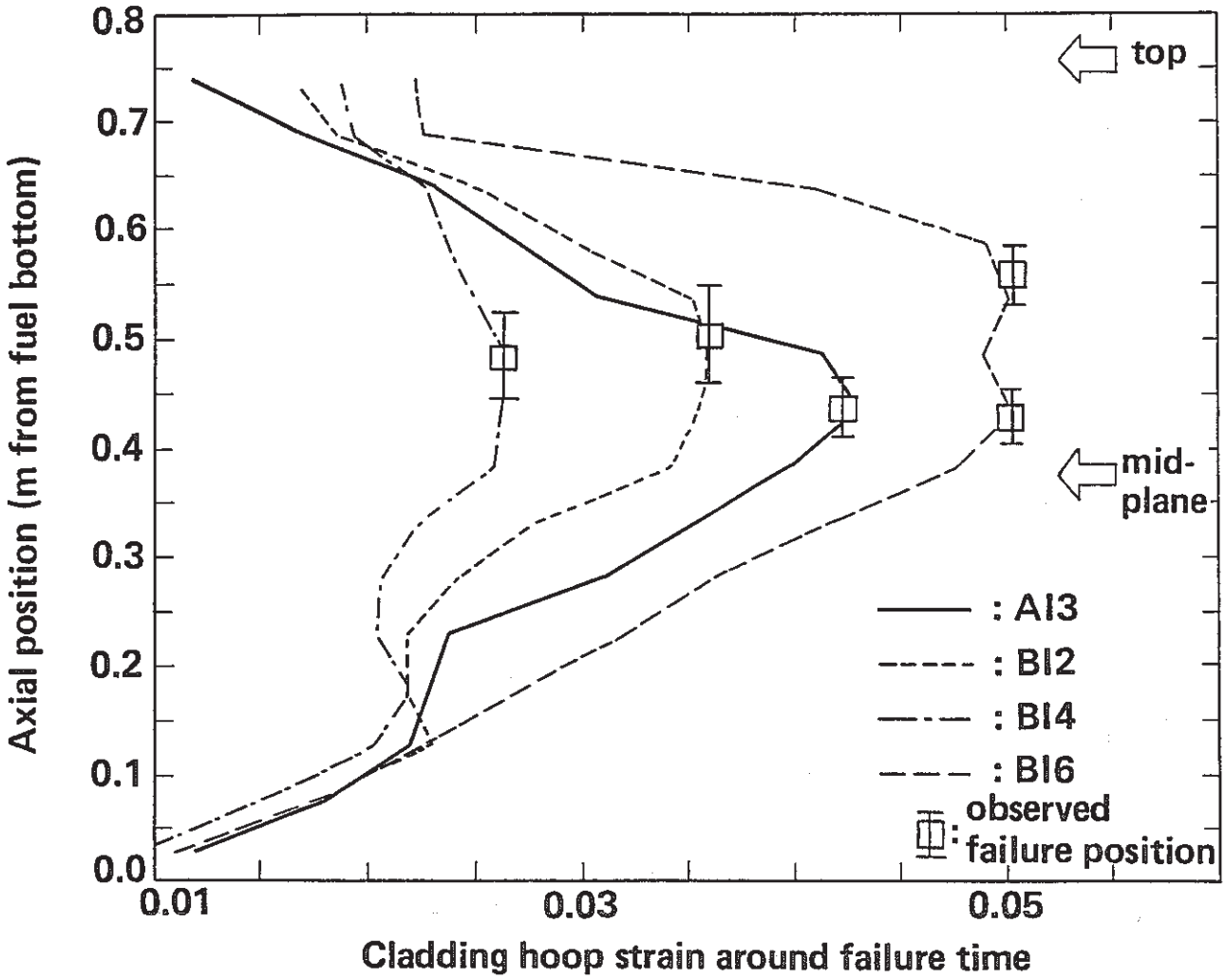

Fig.10 Axial strain profiles predicted by PAPAS–2S and observed failure positions

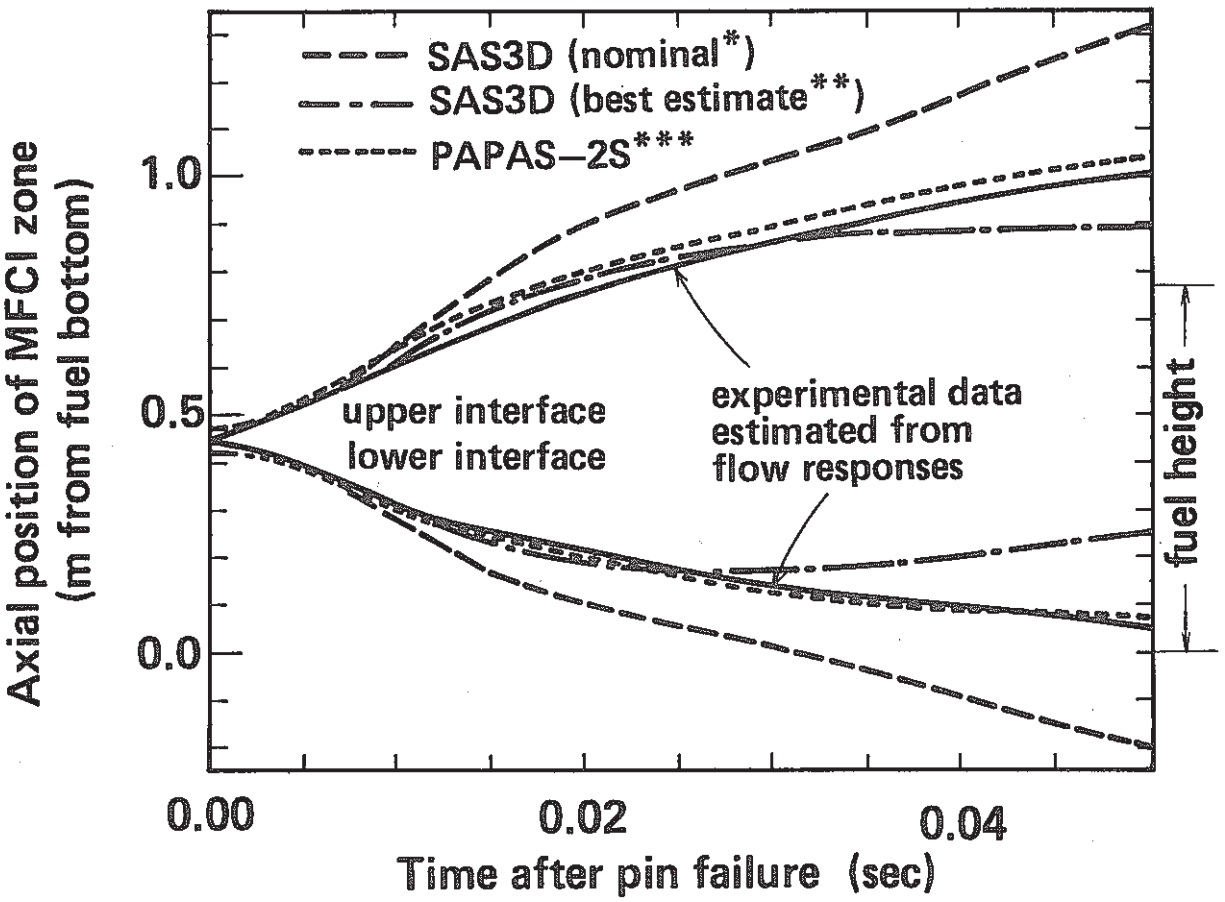

* mixing time constant t_m : 5 ms
** t_m : 0.1 ms, enhanced blanketing : 4 ms after failure
*** t_m : 0.1 ms, no failure propagation

Fig. 11 MFCI zone expansion behaviours in AI3 test analyses

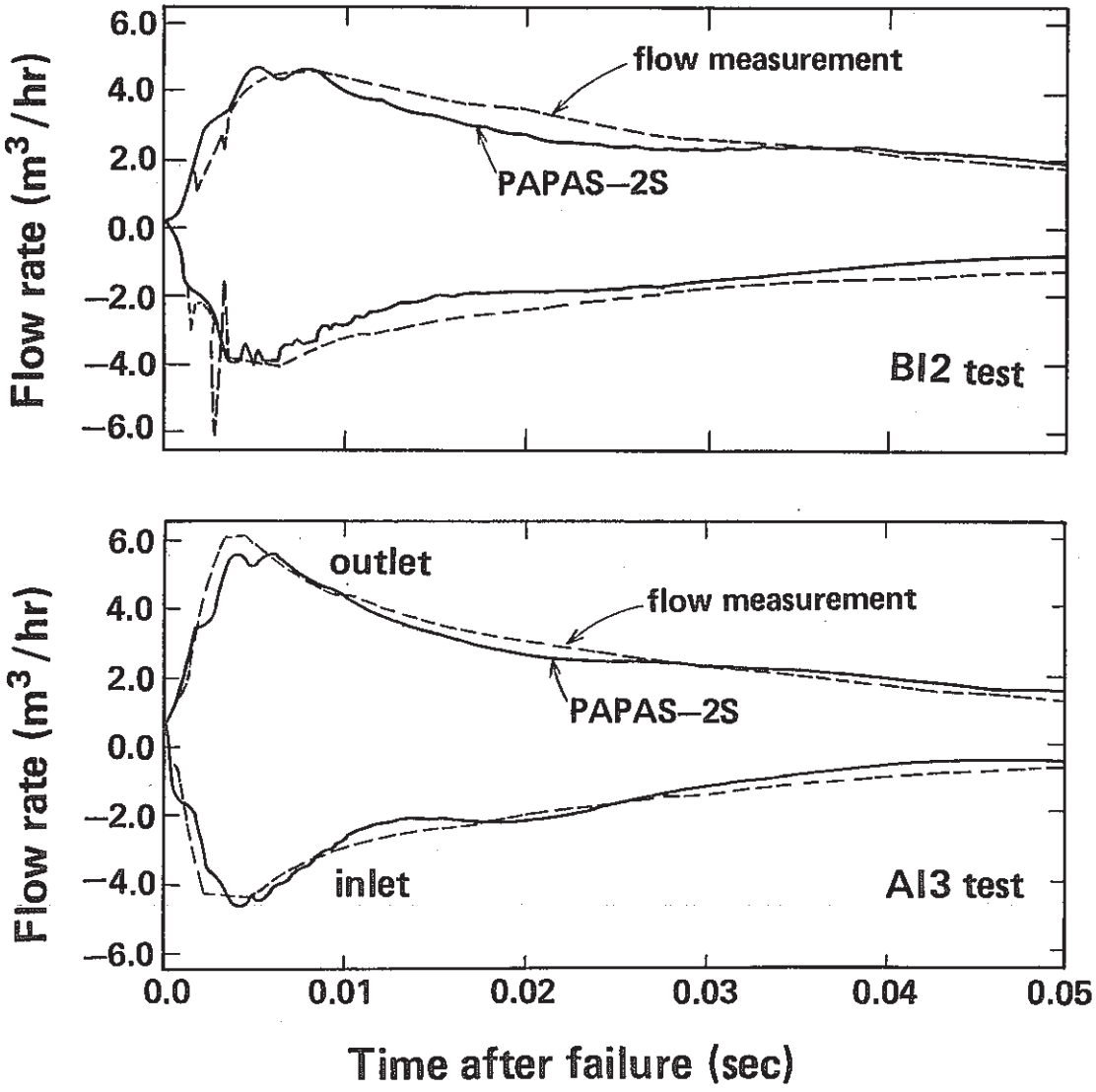

Fig. 12 Flow transients in AI3 and BI2 tests

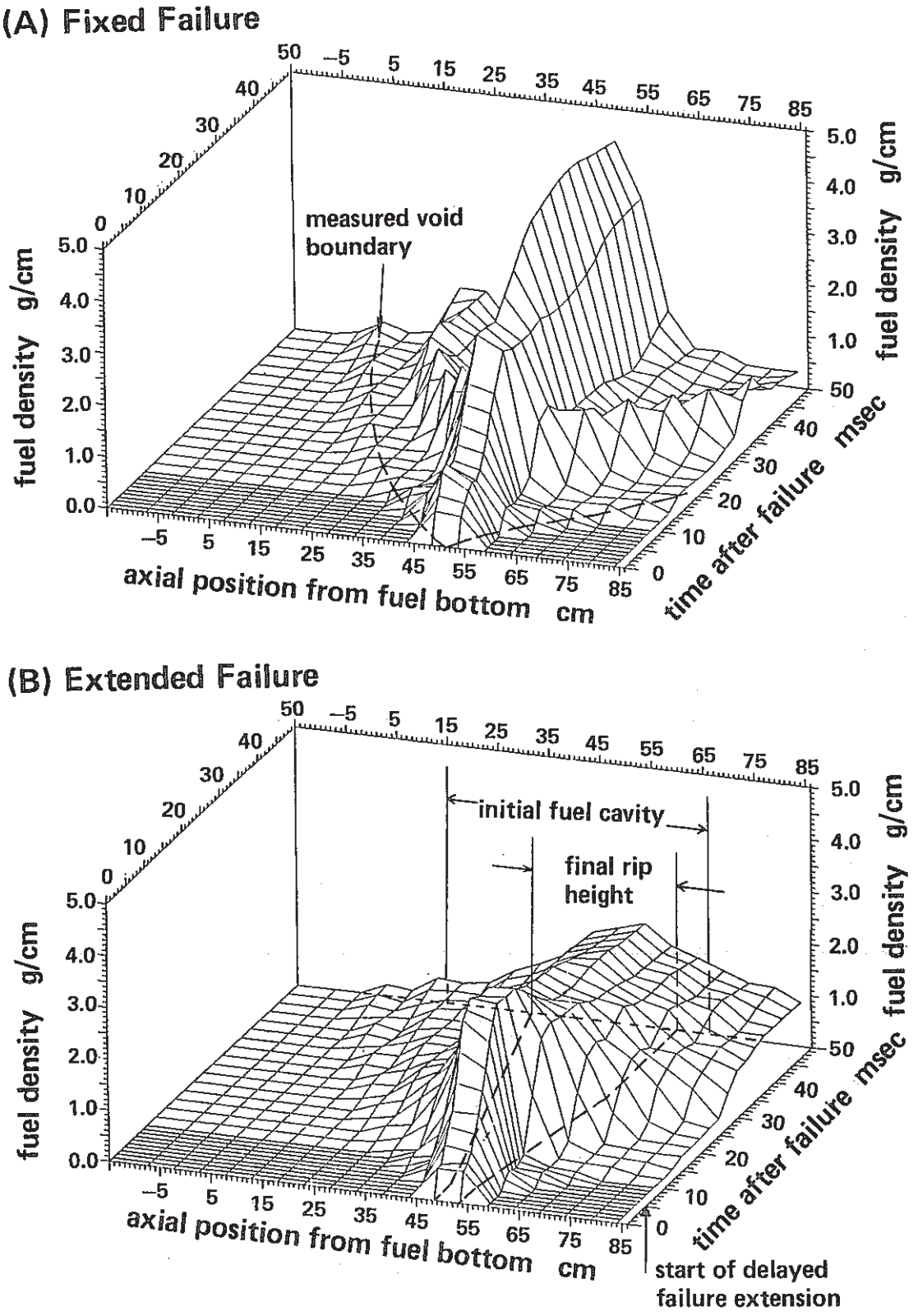

Fig. 13 Effect of failure extension on fuel motion in coolant channel : PAPAS–2S analyses of BI2 test

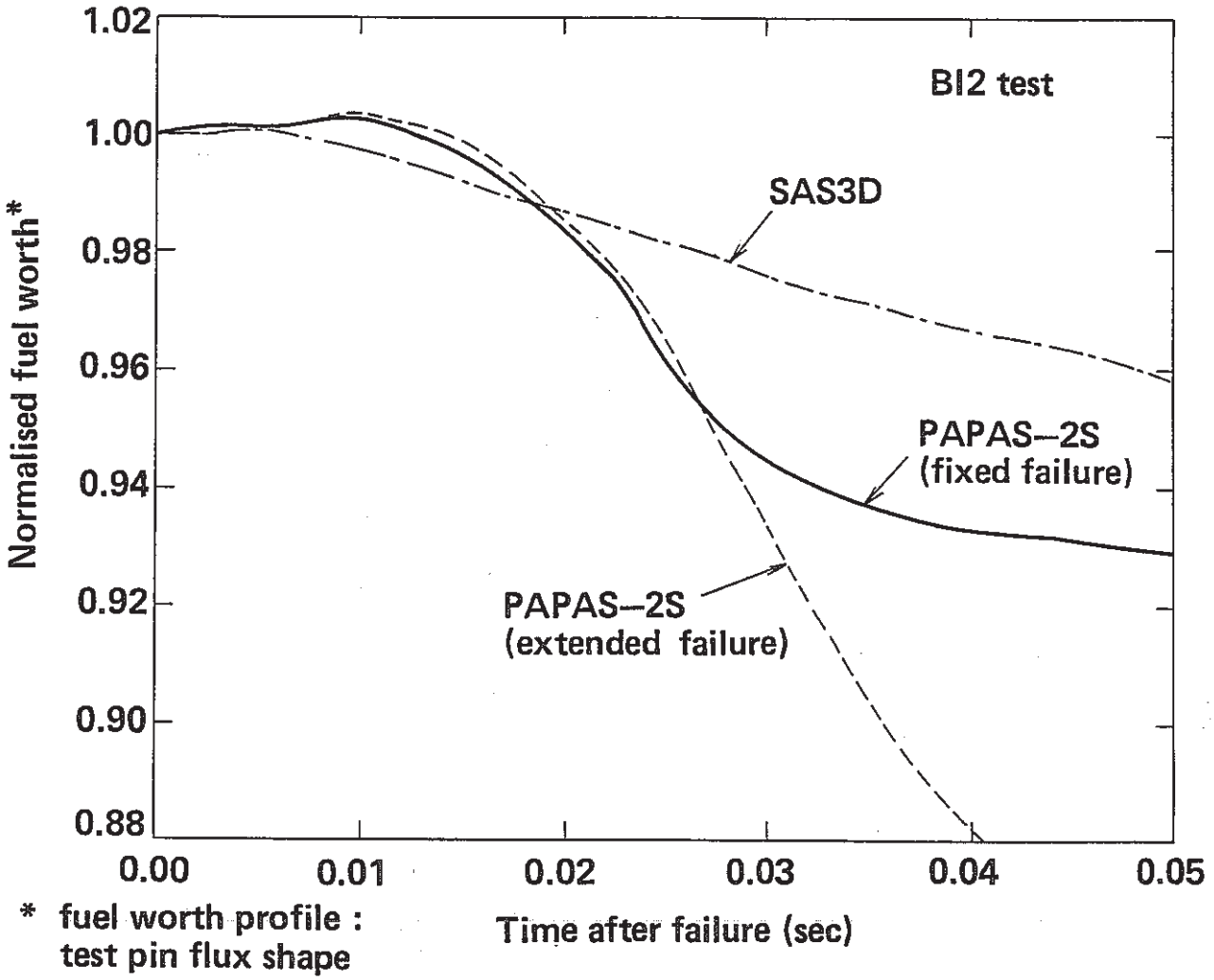

Fig. 14 Histories of fuel worth change in BI2 test analyses